

Chalmers Publication Library



This is an author-created, un-copyedited version of an article accepted for publication in *Journal of Physics: Condensed Matter*. IOP Publishing Ltd is not responsible for any errors or omissions in this version of the manuscript or any version derived from it. The definitive publisher authenticated version is available online at <http://dx.doi.org/10.1088/0953-8984/23/17/175401>.

(Article begins on next page)

Neutron Total Scattering Study of Local Coordination in KTiOPO_4 , from Room Temperature to 900°C

Stefan T. Norberg^{1,2}, Pamela A. Thomas³ and Matthew G. Tucker²

¹ Department of Chemical and Biological Engineering, Chalmers University of Technology, SE-412 96 Gothenburg, Sweden

² The ISIS Facility, Rutherford Appleton Laboratory, Didcot, Oxfordshire, OX11 0QX, United Kingdom

³ Department of Physics, University of Warwick, Coventry CV4 7Al, United Kingdom

Corresponding author:

Stefan Tommy Norberg

Department of Chemical and Biological Engineering

Chalmers University of Technology

SE-412 96 Gothenburg, Sweden

E-mail: stn@chalmers.se

Phone: +46 31 7722866

Fax: +46 31 7722853

Keywords: RMC modelling, neutron total scattering, local cation ordering, nonlinear optical material

Short title: Neutron total scattering study of local coordination in KTiOPO_4

PACS Numbers: 61.05.fm Neutron Diffraction
64.60.Cn Order-disorder transformation

Abstract

Neutron total (Bragg plus diffuse) scattering data have been analyzed with bond valence constrained reverse Monte Carlo (RMC), using the *RMCPProfile* software, in order to simultaneously probe the nature of the short- and long-range structural correlations in potassium titanyl phosphate, KTiOPO_4 (KTP). The diffraction data has been collected at room temperature, 300°C , 500°C , 700°C and 900°C and the resulting partial radial distribution functions, $g_{jk}(r)$, has been thoroughly investigated for information about the structural aspects that cause a reduced second harmonic generation (SHG) with increasing temperature in KTP. The $-\text{TiO}_6\text{-PO}_4-$ lattice show very little rigid unit motion up to 900°C and the PO_4 tetrahedra was likewise unchanged. However, subtle changes regarding oxygen disordering around the TiO_6 octahedra, *i.e.* the amount of short titanyl bonds, and K^+ cation displacement along the c axis is carefully mapped out. The later has a direct detrimental effect on the SHG response, whilst the anisotropic Ti-O bond distribution seems to be a prerequisite for the SHG effect.

1. Introduction

Potassium titanyl phosphate, KTiOPO_4 (KTP), is a well known ferroelectric nonlinear optical (NLO) material used for frequency conversion [1], especially for applications that utilize the second harmonic generation (SHG) effect for laser-frequency doubling [2]. KTP has a non-centrosymmetric structure with highly asymmetric bonds [3], most notably both crystallographically-independent TiO_6 octahedra contain one anomalously short Ti-O bond, of length $< 1.78 \text{ \AA}$, while the remaining Ti-O bonds are in the range of 1.93 to 2.13 \AA . The TiO_6 octahedra are corner-linked by alternating *cis*- and *trans*-coordination, and the resulting Ti-O chains are bridged by PO_4 tetrahedra, forming an open network structure with the K^+ cations in cavities connected by channels oriented along the *c*-axis, see figure 1.

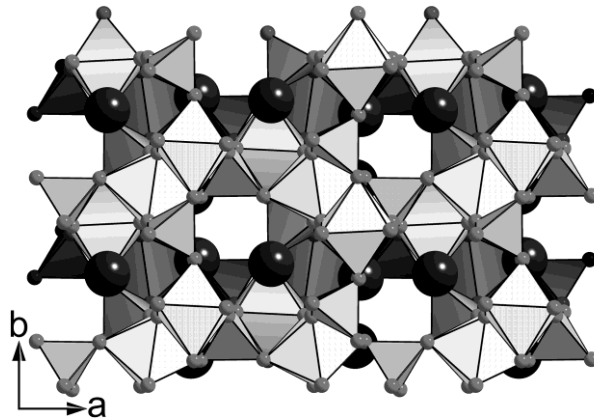


Figure 1 The KTP structure viewed along $[001]$, with P^{5+} and Ti^{4+} located inside oxygen tetrahedra and octahedra, respectively, and the K^+ cations in the structural cavities.

The transparent crystal has favourable material properties, such as a high thermal and chemical stability, and a high optical nonlinearity with a wide transmission window that covers both the UV and IR spectra. These properties are also found in some isostructural ATiOBO_4 compounds, particularly for those with $A = \text{K, Rb, Cs}$ or Tl and $B = \text{P}$ or As . In fact, the last 25 years have seen a great effort towards crystallization of isostructural analogues of KTP, (see for example reviews [4] and [5], and references therein). These isostructures have often been candidates for improved physical properties, *e.g.* the optical transmission range and absorption, although frequently, despite their similar crystal structures, the NLO properties are inferior to those of KTP itself. The

KTP structure has at room temperature (RT) a strong degree of pseudosymmetry, which points to the high-temperature phase, with symmetry $Pnan$, as argued by Thomas *et al.* [6-7] and observed experimentally for the Tl analogues by Harrison *et al.* [8-9]. The phase transition Curie temperature (T_C) is usually close to 945°C [10-11], although the actual T_C can vary widely depending on crystal growth conditions, thermal treatment and the number of K^+ vacancies, and has been reported to be as low as 883°C [12].

The ferroelectric to paraelectric phase transition of the KTP family is described as being of continuous second order and is both displacive and of order-disorder nature [13]. Recently, Yashima & Komatsu have reported [14] a high-temperature neutron powder diffraction study of KTP up to 1085°C, which briefly describes a Rietveld refinement of the structure of the $Pnan$ phase. The structural model includes split K^+ sites as evidence of the order-disorder nature, with the high-temperature position of the K^+ being divided over two sites equivalent by n -glide symmetry and each having approximately 50% occupancy. The major displacive component of the phase transition is a continuous shift of the K^+ sites, most notably along the c -axis [6-7, 15-16], whilst the order-disorder components are due to the K^+ split sites whose occupancy factor increase with increasing temperature [14-15]. The first indication of alkali cation disorder among the KTP isostructures was the detection of residual electron density peaks in the vicinity of the K^+ cation sites in $KFeFPO_4$ single crystals [17], and subsequently the position and occupancy of similar alkali split sites has been determined for KTP at RT [18-19]. Altogether, a large number of KTP isostructures, *e.g.* $RbTiOPO_4$ [20], $(Cs,Rb)TiOAsO_4$ [21], and $Rb(Ti,Ge)OPO_4$ [22], have been studied in an effort to understand the nature of the disorder on the alkali cation sites, and most of these studies support the existence of split alkali sites. However, an alternative to the split-site model is the use of an anharmonic displacement model [23-24] and there is also some question about the reliability of the refined split-site occupancies [25]. Nevertheless, it is important to note that all of the above-mentioned structural models are based on measurement and refinement against only the Bragg scattering and contains only long-range correlations, *i.e.* the average unit cell, and that information about short-range structural correlations are needed to improve the existing models describing the alkali cation disorder and its influence on the ferroelectric phase transition.

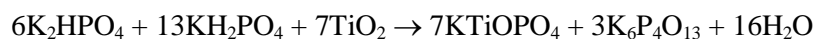
The origin of the high NLO response in KTP crystals is likewise not determined with any certainty, although theories do exist. The first plausible model focused on the short Ti-O titanyl bonds [6, 26], where the bond-polarizability model of Levine [27] indicated the titanyl bonds to be the key requirement for NLO in KTP. This interpretation was supported by early charge density studies that found an excess of electron density along the short Ti-O bonds [28], signifying a covalent character with high bond polarizability. It was also observed that KSnOPO_4 with its less distorted octahedral bonds has a SHG response of about 2% of KTP [6]. Additional substitution studies, this time exchanging K^+ for Na^+ , threw some doubt on the above model since the TiO_6 octahedra are as distorted as for KTP, but the NLO response is reduced by a factor of 10 [29]. It was furthermore revealed that the optical nonlinearity of KTiOAsO_4 (KTA) is larger than that for KTP, even though their TiO_6 octahedra are very similar, and the increased NLO response was explained by the greater polarizability of As^{5+} in comparison with P^{5+} [30]. More recent updated bond polarizability calculations state that the main source of the high optical nonlinearity in KTP and KTA is the PO_4 (AsO_4) tetrahedra and the polarizability of the K-O bonds [31], a statement that contrasts with earlier studies. In an effort to examine more closely the bonding environments of the key ions in the structure, Thomas *et al.* [32] performed a ^{17}O , ^{39}K , and $^{47,49}\text{Ti}$ solid-state NMR investigation to study ion-pair correlations in KTP at RT. The result unequivocally indicated that the character of the short Ti-O bonds is mainly ionic, thus dismissing the earlier theory that covalent charge localized in these bonds is the key to nonlinearity but also explaining that the geometrical distortion of the octahedra was still required, *i.e.* the presence of highly-distorted octahedral is necessary but not sufficient for enhanced nonlinearity. This interpretation, which also used new *ab initio* DFT studies in support of the model, agrees with recent bond polarizability calculations [31] and with all the observations to date regarding relative nonlinearity displayed by the different KTP isomorphs in the experimental studies discussed above. It should be noted however, that this study considered the local structure of KTP only at RT and no consideration was given to disorder on the K^+ sites or elsewhere in the structure – indeed, there was no evidence from the NMR spectra that disorder should be invoked. To evaluate the effects of local structural disorder on the structure, optical properties and ferroelectric phase transition of KTP, examination by an alternative technique, such as an ion-ion pair distribution analysis, is necessary.

Thus, in this paper we report the result of a variable temperature neutron diffraction study of KTP, from RT up to 900°C, evaluating the diffraction data using both Rietveld refinement [33] and reverse Monte Carlo (RMC) modelling [34-35]. The former method focuses solely on the Bragg scattering and provides time-averaged long-range structural models, whilst the latter technique analyzes the total (*i.e.* Bragg and diffuse) scattering to simultaneously investigate both short- and long-range ion-ion correlations. Temperature related trends in the TiO₆ octahedra and PO₄ tetrahedra, as well as the K⁺ cation distribution are evaluated and linked to the ferroelectric to paraelectric phase transition and changes in the nonlinear optical properties.

2. Experiments and Structure Modelling

2.1. Sample Preparation

Crystals of KTP were grown by spontaneous nucleation from a self-flux, a method adapted from that of Jacco *et al.* [36]. Analytical-grade starting chemicals were weighed out according to the reaction:



The powders were mixed thoroughly and placed in a 25cm³ platinum crucible, which in turned was heated up to 1100°C in a furnace. The solution was held at this soak temperature for 12 hours before being cooled at 5°C per hour to 700°C and then undergoing natural cooling to RT. The colourless crystals formed were typically ~0.1-1 mm in maximum dimension. They were recovered from the remaining flux by washing in hot de-ionized water. The crystals were ground by hand and then placed in an automatic grinding system, which utilizes agate pellets as fine-grinding medium. A free-flowing powder was produced as a result of this procedure. A sample of the powder was mounted on a PANalytical powder diffractometer for phase identification, which showed the presence of only the expected KTP phase.

2.2. Neutron Powder Diffraction

Neutron diffraction experiments were performed using the Polaris diffractometer at the ISIS facility, Rutherford Appleton Laboratory, U.K. [37], using the backscattering detector bank (covering scattering angles of $130^\circ < 2\theta < 160^\circ$, giving a d -spacing range of $0.2 < d(\text{\AA}) < 3.2$, with a resolution of $\Delta d/d \sim 5 \times 10^{-3}$), the 90° detector bank ($85^\circ < 2\theta < 95^\circ$, $0.3 < d(\text{\AA}) < 4.1$, $\Delta d/d \sim 7 \times 10^{-3}$), and the low angle detector bank ($28^\circ < 2\theta < 42^\circ$, $0.5 < d(\text{\AA}) < 8.3$, $\Delta d/d \sim 10^{-2}$). The KTP powder was encapsulated in a cylindrical 6 mm diameter thin-walled (40 μm) vanadium can, and subsequently placed in a furnace designed for neutron diffraction studies constructed of vanadium foil resistive heat elements and heat shields. The diffraction data used for the RMC modelling were collected at RT, 300°C, 500°C, 700°C and 900°C for a minimum of 12 hours each, with additional Rietveld quality data collected at intervals of 50°C. KTP is known to start decompose at temperatures near the phase transformation and, after cooling, an additional 1 hour of neutron diffraction data was collected and it was determined that the crystallinity of the KTP sample was not affected during the long 900°C measurement.

2.3. Neutron Total Scattering

For the total scattering, diffraction data gathered from all Polaris detector banks were merged to cover a wide d -spacing which in turn is corrected for background scattering and beam attenuation using the program *Gudrun* [38], which also puts the scattered intensities onto the absolute scattering cross-section scale required for subsequent RMC modelling. The normalized total scattering structure factors, $S(Q)$, were thereafter used to generate the corresponding total pair distribution functions, $G(r)$, via a Fourier transform

$$G(r) = \frac{1}{(2\pi)^3 \rho_0} \int_0^\infty 4\pi Q^2 S(Q) \frac{\sin Qr}{Qr} dQ, \quad (1)$$

ρ_0 is the average atom number density (in atoms \AA^{-3}), and the scattering vector Q is related to the interplanar spacing, d , with $Q = 2\pi/d$. The total pair distribution function, $G(r)$, can also be expressed in terms of the individual partial pair distribution functions, $g_{ij}(r)$, weighted by the concentrations of the two species, c_i and c_j , and their neutron scattering lengths, b_i and b_j , so that

$$G(r) = \frac{\sum_{i,j=1}^n c_i c_j \bar{b}_i \bar{b}_j g_{ij}(r)}{\sum_{i=1}^n (c_i \bar{b}_i)^2}. \quad (2)$$

The partial pair distribution function is in turn given by

$$g_{ij}(r) = \frac{1}{4\pi r^2 dr} \frac{n_{ij}(r)}{\rho_j}. \quad (3)$$

With $n_{ij}(r)$ equal to the number of atoms of type j located at a distance between r and $r + dr$ from an atom of type i and ρ_j is the number density of atoms of type j , given by $\rho_j = c_j \rho_0$. These individual partial distribution functions, $g_{ij}(r)$, can be obtained from RMC modelling, which simultaneously probes both the long- and short-range structural properties. See Keen [39] for additional information regarding the total scattering formalism.

2.4. Reverse Monte Carlo Modelling

Analysis of the neutron total scattering data (Bragg peaks plus diffuse scattering components) was performed with bond valence sum (BVS) constrained RMC modelling using the *RMCPProfile* software [40-41]. The BVS added RMC methodology has shown to be very useful to keep the individual ion-ion coordination environments chemically reasonable, see for example the recent total scattering study on the $\text{Zr}_2\text{Y}_2\text{O}_7\text{-Y}_3\text{NbO}_7$ system [42], and hence keep the K^+ cations to chemically sensible coordination environments. Of great importance for obtaining the relevant short-range ion pair correlations in KTP are the neutron scattering weight factors, $c_i c_j \bar{b}_i \bar{b}_j$, related to the TiO_6 octahedra, PO_4 tetrahedra and K-O coordination, with values of -0.03117, 0.04652, and 0.03327 for $g_{\text{TiO}}(r)$, $g_{\text{PO}}(r)$, and $g_{\text{KO}}(r)$, respectively. This gives the RMC modelling a similar sensitivity to each $g_{\text{Cation-O}}(r)$. Note also that the negative scattering weight factor for $g_{\text{TiO}}(r)$ will cause a negative contribution to the total $G(r)$, thus making the short-range Ti-O bond distance distribution distinctly visible in $G(r)$ plots.

Each RMC model, one for each temperature, used a configuration box of $6 \times 8 \times 6$ unit cells, *i.e.* a box containing a total of 2304 K^+ , 2304 Ti^{4+} , 2304 P^{5+} , and 11520 O^{2-} , with all ions initially distributed at their regular crystallographic sites. The BVS parameters used for the soft BVS constraint [41] were all taken from Brese & O'Keefe [43], and the ensuing RMC modelling was fitted using reciprocal space data, $S(Q)$, and real space data, $G(r)$. The former is broadened by convolution with a box function to reflect the finite size of the configuration box, where

$$S_{\text{box}}(Q) = \frac{1}{\pi} \int_{-\infty}^{\infty} S_{\text{expt}}(Q') \frac{\sin L(Q-Q')/2}{Q-Q'} dQ'. \quad (4)$$

L is the smallest dimension of the RMC configuration and, as such, defines the upper limit of the $G(r)$. The broadened $S_{\text{box}}(Q)$ is used in the RMC modelling, and the comparison between the calculated functions and the experimental data is defined by an agreement factor

$$\chi_{RMC}^2 = \sum_j \chi_j^2, \quad (5)$$

where χ_j^2 is the individual agreement factor for data type j . Changes within the RMC configuration box which result in a reduction of χ_{RMC}^2 are accepted, whilst others are accepted with a probability of $\exp(-\Delta\chi_{RMC}^2/2)$ until, on average, no further improvement of χ_{RMC}^2 is observed. The quality of the final fit to both the $S_{\text{box}}(Q)$ and the $G(r)$ for KTP at RT and 900°C is shown in figures 2 and 3, respectively. In this way 10 independent configurations were generated for each total scattering data set.

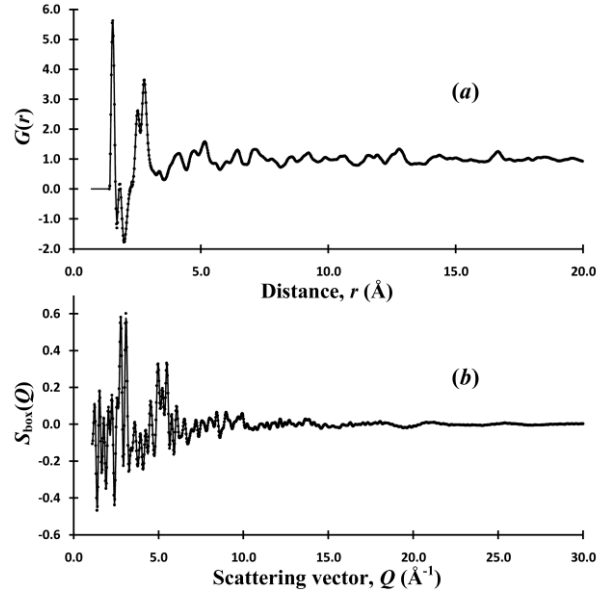


Figure 2 The (a) $G(r)$ and (b) $S_{\text{box}}(Q)$ fits obtained by the RMC modelling of the KTP neutron diffraction data collected at RT, with dots showing the experimental data and the solid line showing the calculated profile.

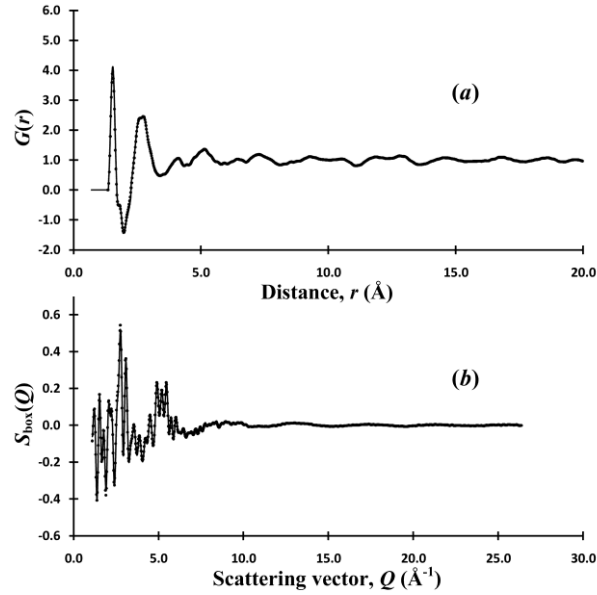


Figure 3 The (a) $G(r)$ and (b) $S_{\text{box}}(Q)$ fits obtained by the RMC modelling of the KTP neutron diffraction data collected at 900°C, with dots showing the experimental data and the solid line showing the calculated profile.

3. Results & Discussion

3.1. Average Structure from Rietveld Refinements

The long-range average structure models were refined with the Rietveld method, as illustrated in figure 4, using the GSAS software [44] and initial K/Ti/P/O atomic positions as described in reference [45]. The refined parameters consisted of a scale factor, an extinction factor, orthorhombic lattice parameters, a , b , c , atomic coordinates, an isotropic thermal vibration parameter for each atomic specie, u_{K} , u_{Ti} , u_{P} , and u_{O} , plus 36 coefficients of a shifted Chebyshev polynomial describing the undulating background scattering and 2 coefficients describing Gaussian and Lorentzian contributions to the Bragg peak shapes. Excellent fits were obtained throughout the whole series of measurements and changes in lattice and thermal vibration parameters with increasing temperature are plotted in figure 5, whilst table 1 & 2 report crystallographic parameters and fractional coordinates for KTP at RT and 900°C. The substantially enlarged thermal vibration parameter with elevated temperature for the K^+ cations indicates a considerably increased disorder around the Rietveld determined sites. This is in contrast to the Ti^{4+} cations that seem to be regularly positioned throughout the KTP

crystal, irrespectively of temperature. However, this Rietveld analysis focuses solely on the Bragg reflections and the structural model is therefore averaged over time and all the unit cells within the sample. It is, therefore, highly advantageous to directly probe the short-range ion-ion correlations, and neutron total scattering data that includes both the Bragg scattering and the diffuse scattering components have been analyzed with the RMC method to that effect.

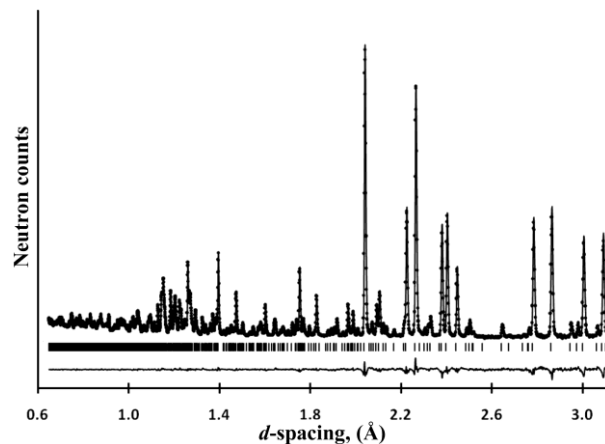


Figure 4 The Rietveld fit for the KTP neutron diffraction data collected at RT with dots indicating the experimental data and the solid line the calculated profile. The short vertical lines indicate allowed Bragg reflections (space group $Pna2_1$), and the difference between the observed and calculated data is plotted at the bottom.

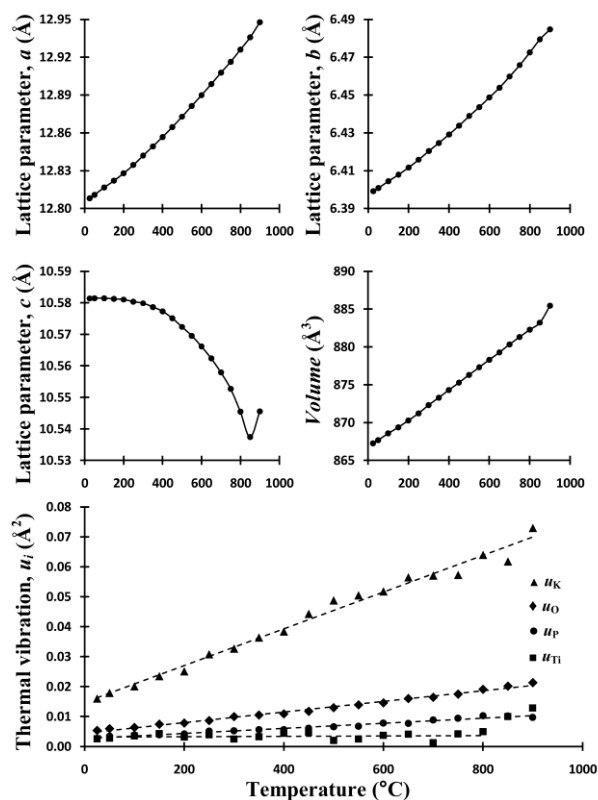


Figure 5 Measured temperature dependence for unit cell parameters a , b , c and the unit cell volume, plus refined changes in isotropic thermal vibration for the K^+ , Ti^{4+} , P^{5+} and O^{2-} ions. The standard uncertainties, for all data points, are smaller than the symbols used to indicate determined values.

3.2 Pair Distribution Functions

All experimentally measured total pair distribution functions are plotted in figure 6, and the temperature dependence of the short-range ion-ion correlations for partial pair distribution functions $g_{\text{PO}}(r)$ and $g_{\text{TiO}}(r)$ are easily observed. The first $G(r)$ peak with its maxima near 1.54 \AA is the P-O bond distance distribution in the PO_4 tetrahedra and the subsequent part of the $G(r)$ functions, between ~ 1.66 and 2.28 \AA , having a negative value due to the negative neutron scattering length of Ti, describes the Ti-O bond distance distribution in the TiO_6 octahedra.

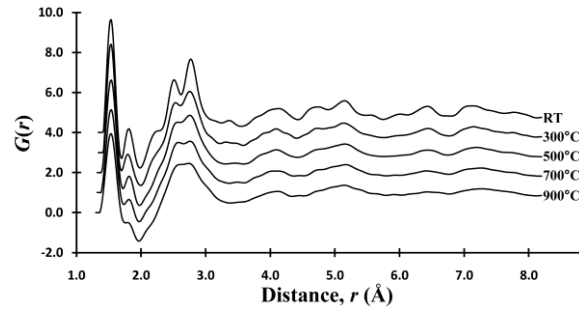


Figure 6 Experimental total pair distribution functions, $G(r)$, as calculated by Fourier transform of the collected total scattering data.

Figure 7 plots the temperature dependence of the short-range region of the RMC extracted partial pair distribution functions $g_{\text{PO}}(r)$, $g_{\text{TlO}}(r)$, $g_{\text{OO}}(r)$ and $g_{\text{KO}}(r)$, that are all of importance for correlating the KTP structure with physical properties. It is readily observed that the first $g_{\text{PO}}(r)$ peak, see figure 7(a), only undergoes a slight broadening with increasing temperature and the PO_4 tetrahedra is thus very stable up to 900°C. The small amount of $g_{\text{PO}}(r)$ peak broadening is from increased thermal vibration, and the slight increase in the average P-O bond distance, from 1.536 Å to 1.538 Å, corresponds well with the Rietveld determined structural model. However, the remaining pair distribution functions, $g_{jk}(r)$, plotted in figure 7 exhibit temperature dependent features not only related to increasing thermal vibration, but also from structural changes and local disorder.

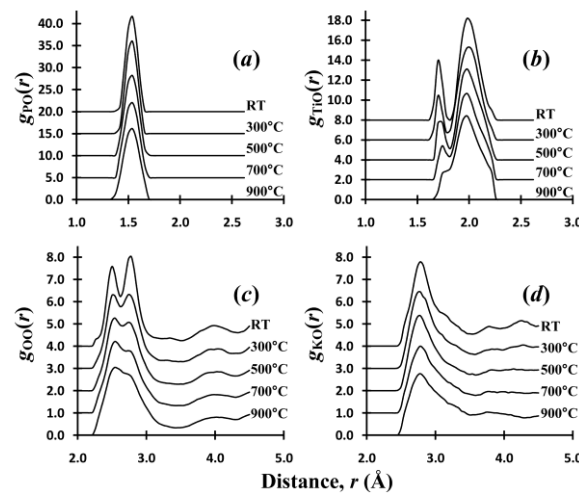


Figure 7 Temperature dependence of partial pair distribution functions (a) $g_{\text{PO}}(r)$, (b) $g_{\text{TlO}}(r)$ (c) $g_{\text{OO}}(r)$ and (d) $g_{\text{KO}}(r)$ as extracted from RMC modelling of neutron total scattering diffraction data.

Significantly, the oxygen coordination around the Ti^{4+} cations change considerably with increased temperature, see figure 7(b), and it should be noted that changes in such a complex bond distance distribution is not possible to quantify using average structural data from Bragg peak refinement. The $g_{\text{TiO}}(r)$ have two clearly visible Ti-O bond distribution peaks for all measurements at temperatures below 900°C. The first peak at ~ 1.70 Å gives the bond distance distribution of the short titanyl bonds, and the second peak centred roughly at 1.99 Å describes the distribution of the remaining Ti-O bond distances. Calculation of the titanyl bond fraction, defined herein as being Ti-O bond distances ≤ 1.80 Å, suggest that KTP have roughly 16.1% titanyl bonds at RT which corresponds extremely well with the existing low temperature model, *i.e.* that each TiO_6 octahedra have one anomalously short Ti-O bond.

The $g_{\text{OO}}(r)$ have two distinct short coordinating distances at RT, see figure 7(c), with a first peak at ~ 2.50 Å due to O-O coordination around the PO_4 tetrahedra, and a second peak at ~ 2.77 Å from O-O coordination around the TiO_6 octahedra. The $g_{\text{OO}}(r)$ peak at 2.50 Å is only slightly reduced with increasing temperature, whilst the considerable temperature related changes for the $g_{\text{OO}}(r)$ peak at 2.77 Å indicate a significantly increased O^{2-} anion disorder around the Ti^{4+} cation sites with increasing temperature. The $g_{\text{KO}}(r)$, see figure 7(d), seems deceptively unchanged with increased temperature but a careful study of the K-O coordination environment, see table 3, reveal a continuous and subtle cation positional shift with increased temperature. The average coordination number decrease from 7.94 to 7.36 oxygen cations, whilst the average K-O bond distance increases from 2.890 to 2.911 Å. This shift of K^+ cation position is visualized in section 3.5.

3.3 Angular Distribution Functions & Geometric Analysis

The temperature dependence of the angular distribution functions, $A(\theta)$, can be extracted from the RMC models and selected structurally representative bond angle functions is shown in figure 8. As expected, the $A_{\text{OPO}}(\theta)$, figure 8(a), indicate a stable O-P-O bond angle distribution that is not affected by the change from RT to 900°C. However, less expected is that the $A_{\text{OTiO}}(\theta)$, figure 8(b), hardly changes with increasing temperature even though

the Ti-O bond distribution changes with increasing temperature, see figure 7(b), indicating a substantial stability of the TiO_6 octahedra shape.

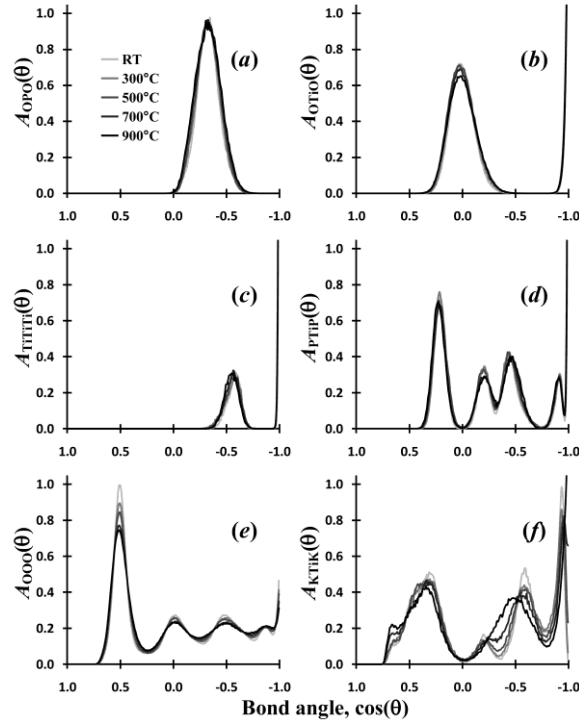


Figure 8 Temperature dependence of angular distribution functions (a) $A_{\text{OPO}}(\theta)$, (b) $A_{\text{OTiO}}(\theta)$, (c) $A_{\text{TiTiTi}}(\theta)$, (d) $A_{\text{PTiP}}(\theta)$, (e) $A_{\text{OOO}}(\theta)$ and (f) $A_{\text{KTiK}}(\theta)$ as extracted from RMC modelling of neutron total scattering diffraction data.

The overall stability of the $-\text{TiO}_6\text{-PO}_4-$ lattice can be evaluated by angular distribution functions $A_{\text{TiTiTi}}(\theta)$ and $A_{\text{PTiP}}(\theta)$, see figure 8(c) and (d), representing the chains of linked TiO_6 octahedra that are bridged by PO_4 tetrahedra. Both the $A_{\text{TiTiTi}}(\theta)$ and $A_{\text{PTiP}}(\theta)$ are essentially unchanged throughout the measured temperature interval, with only a slight peak broadening at the higher temperatures, so no large cation displacements takes place in the $-\text{TiO}_6\text{-PO}_4-$ lattice. A more substantial bond angle broadening is seen for the $A_{\text{OOO}}(\theta)$, see figure 8(e), which confirms that the temperature related changes in the $g_{\text{PO}}(r)$ and $g_{\text{TiO}}(r)$ are due to positional shifts and disorder of the O^{2-} anions. However, the most significant angular distribution changes are related to the K^+ cation, as illustrated with the $A_{\text{KTiK}}(\theta)$ in figure 8(f). The low temperature $A_{\text{KTiK}}(\theta)$ have broad peaks around 71° , 101° , 126° , and 159° , whilst the 900°C $A_{\text{KTiK}}(\theta)$ have broad peaks roughly at 70° , 118° and 180° . The measured K-Ti-K bond angle distributions point towards a significant temperature dependence on the K^+ cation positioning

between the helical chains of TiO_6 octahedra, with the RT result agreeing well with the Rietveld refined $Pna2_1$ structure, and the 900°C results being close to an overall centrosymmetric structure for which existing $Pnan$ high temperature models, *e.g.* references [8] and [14], have K-Ti-K bond angles near and equal to 180° .

The RMC configurations were additionally analyzed using the geometric algebra (GA) method described by Wells *et al.* [46]. This analysis evaluates the amount of rigid polyhedra motion of the PO_4 tetrahedra and the TiO_6 octahedra, and then decomposes the remaining polyhedra distortions into bond stretch and bond bending components. Figure 9 shows the results for KTP at each measured temperature and for comparison the results obtained for the SiO_4 tetrahedra in quartz [46]. The initial mismatch score, labelled disorder, results directly from comparing the polyhedra units in two configurations at the same temperature. GA is then used to minimize the mismatch by rotating polyhedra units, all remaining mismatch is then divided between bond bending and stretching. The quartz data shows a marked increase in polyhedra disorder with increased temperature, while the amount of bond bending and stretching remains fairly constant. This is a clear example of a system where rigid polyhedra motion dominates. It is in comparison obvious that the amount of rigid motion for the PO_4 tetrahedra and the TiO_6 octahedra in KTP is a small part of the total disorder and show almost no temperature variation. The polyhedra distortion in KTP is consequently mainly from disordering of individual atoms.

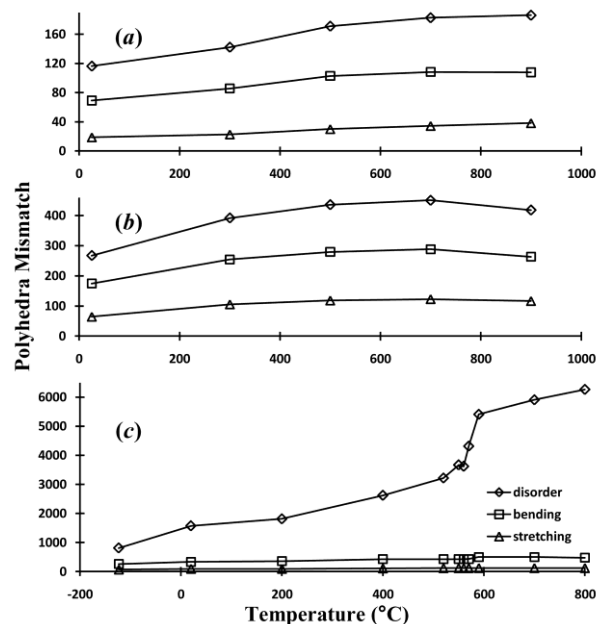


Figure 9 Result of the geometric algebra analysis of the PO₄ tetrahedra and the TiO₆ octahedra, (a) and (b) respectively, in KTP, and for comparison the quartz SiO₄ tetrahedra (c).

3.4 Atom Density Plots

Multiple RMC configurations calculated for each respective temperature have been condensed into atom density plots that cut through the Rietveld determined crystallographic sites for K1 and K2 and whereby visualizes the temperature related changes in the K⁺ cation distribution, see figure 10. An increasing K⁺ cation site disorder along the *c* direction with increasing temperature is clearly visible, as well as an average K⁺ cation displacement. Note that similar plots for the Ti⁴⁺ and P⁵⁺ cation sites, not included for brevity of space, show only normal circular atom density features that are slightly enlarged with increased temperature.

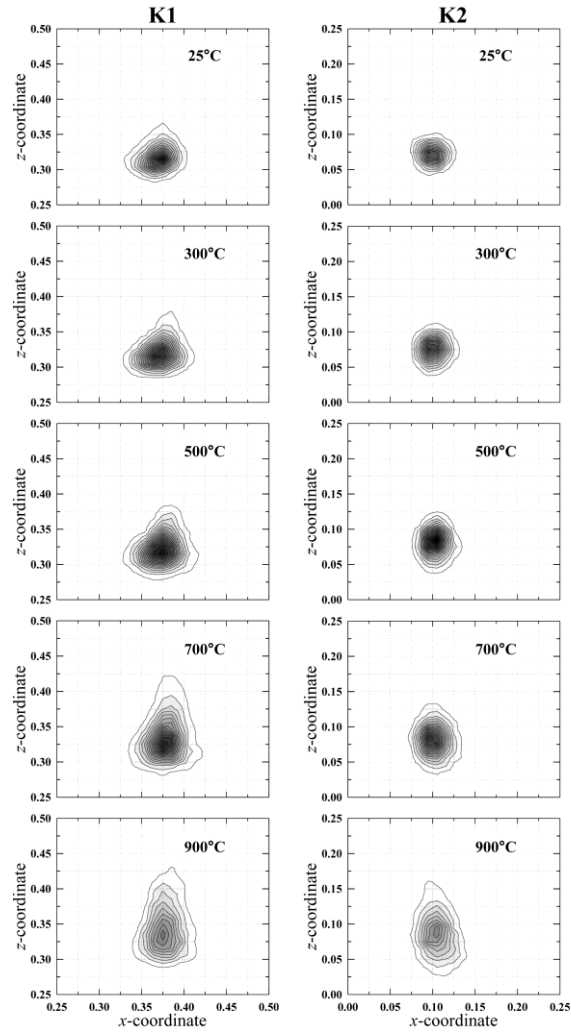


Figure 10 K^+ cation density plots as determined from the RMC modelling.

Previously researchers have approximated this cation distribution with a split site model, based on Bragg peaks measured with single crystal x-ray diffraction, see for example Belokoneva *et al.* (1990) [17], Delarue *et al.* (1999) [15], and Norberg & Ishizawa (2005) [18]. Our model, presented herein, clearly agree with and improve the result of these earlier studies. It is possible to map out the alkali cation distributions with high precision using the results of RMC modelling of very precisely measured total scattering data.

Recently Yashima & Komatsu published an average structural model for the high temperature *Pnan* phase of KTP [14], in which they refined two crystallographically independent K^+ cation sites separated by $\sim 1.03 \text{ \AA}$, and each having roughly a 50% site occupation. An alternative model is to have a single alkali cation site similar to the $TiTiOPO_4$ *Pnan* phase refined by Harrison *et al.* [8], and both these structural models fit well with the RMC

extracted K-Ti-K angular distribution function at 900°C, figure 8(f). Nevertheless, the K^+ cation density distribution plotted in figure 10 indicate that a high temperature model with a single crystallographically independent K^+ cation site, albeit greatly disordered along the c axis, is the preferred structural description of the paraelectric phase.

3.5 Correlation between SHG and $KTiOPO_4$ Structure

The structural stability of the PO_4 tetrahedra, with practically no change in local ordering between RT and 900°C, implies that while their presence might be important for the SHG their disorder is clearly not the cause of the decrease of SHG with increasing temperature in KTP. However, substantial local structural changes are noted for both the K^+ cation distribution and the TiO_6 octahedra. These changes in local ordering can be evaluated in the context of the temperature dependence of the SHG response for KTP, see figure 11, and consequently be used to gain improved knowledge about the structural aspects causing the SHG property. Of great interest for that discussion, see next section, is that the fraction of anomalously short Ti-O bond distances remains at a fairly constant level of ~12% at temperatures from 300°C to 700°C (16.1% at RT), even though the average titanyl bond distance increase from 1.715 Å to 1.745 Å.

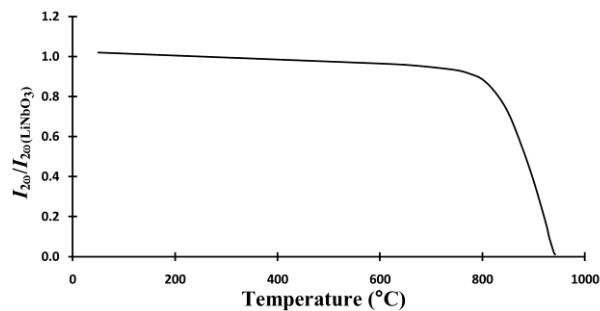


Figure 11 Temperature dependence of the second harmonic generation for KTP crystals, as reported by Sorokina and Voronkova [5].

4. Conclusions

The considerable polyhedra stability $-\text{TiO}_6\text{-PO}_4-$ reported herein indicates that only insignificant lattice deterioration takes place during heating from RT to 900°C , implying that the diminishing SHG response is not due to any polyhedra reorientation. However, it is very likely that the change in local ordering around the Ti^{4+} and K^+ is the cause for the reduced SHG response. The TiO_6 octahedra have an anisotropic Ti-O bond distribution with a surprisingly stable amount of short titanyl bonds between 300°C and 700°C . In fact, the experimental total pair distribution functions (figure 6) and the $g_{\text{TiO}}(r)$ (figure 7b) determined by the RMC analysis indicate only a substantial TiO_6 octahedra deterioration for the 900°C data. Whilst the K^+ cations, between 300°C to 700°C , are increasingly displaced along the c axis, see figure 10 and table 3. With a significant K^+ cation displacement towards a $Pnan$ ordering is taking place above 700°C . This suggests that the slight reduction of SHG up to 700°C is mainly due to the K^+ cation displacement, although one must be careful not to rule out temperature dependent ferroelectric fluctuations due to the Ti-O bond distribution. The greatly diminishing SHG response above 800°C is caused by a combination of TiO_6 octahedra changes, mainly a significant reduced amount of titanyl bonds, and an increased average K^+ cation shift towards a non-centrosymmetric structure.

The previous reports regarding the necessity of the TiO_6 octahedra for an enhanced NLO effect, see the introduction, is thus well supported by the above hypothesis. Additionally, the likely relationship between the K^+ cation displacement, see table 3 and figure 10, and the reduced SHG efficiency between RT and 700°C , see figure 11, strongly suggest that a significant part of the SHG effect is due to the K^+ cations.

The above statements conclude our findings regarding the KTP structural aspects that cause a diminishing SHG response with increasing temperature. However, we also like to use this opportunity to emphasize the general usefulness of analyzing total scattering data with the RMC method [35]. This study provides a good example of investigating a fairly complex structure using experimental data to obtain all partial radial distribution functions. The later can in turn be used as a basis for computer simulations, see for example the work on Bi_2O_3 by Mohn *et al.* [47].

Acknowledgements

The authors would like to thank Stephen Hull (ISIS) for assistance with the RMC analysis. One of the authors (STN) wishes to thank the EU Research and Technology Development Framework Programme for financial support. The ISIS Facility, part of UK Science and Technology Facilities Council, is thanked for allocating beamtime.

List of References

- [1] Zumsteg F C, Bierlein J D and Gier T E 1976 *J. Appl. Phys.*, **47**, 4980-4985
- [2] Boulanger B, Feve J P, Marnier G, Menaert B, Cabirol X, Villeval P and Bonnin C 1994 *J. Opt. Soc. Am. B*, **11**, 750-757
- [3] Tordjman I, Masse R and Guitel J C 1974 *Z. Kristallogr.*, **139**, 103-115
- [4] Stucky G D, Phillips M L and Gier T E 1989 *Chem. Mater.*, **1**, 492-509
- [5] Sorokina N I and Voronkova V I 2007 *Crystallogr. Rep.*, **52**, 80-93
- [6] Thomas P A, Glazer A M and Watts B E 1990 *Acta Crystallogr.* **B46**, 333-343
- [7] Thomas P A and Glazer A M 1991 *J. Appl. Crystallogr.*, **24**, 968-971
- [8] Harrison W T A, Gier T E, Stucky G D and Schultz A J 1990 *J. Chem. Soc., Chem. Commun.*, 540-542
- [9] Harrison W T A, Gier T E, Stucky G D and Schultz A J 1995 *Mater. Res. Bull.*, **30**, 1341-1349
- [10] Yanovskii V K and Voronkova V I 1986 *Phys. Status Solidi a*, **93**, 665-668
- [11] Chu D K T and Hsiung H 1992 *Appl. Phys. Lett.*, **61**, 1766-1768
- [12] Angert N, Tseitlin M, Yashchin E and Roth M 1995 *Appl. Phys. Lett.*, **67**, 1941-1943
- [13] Belokoneva E L, Knight K S, David W I F and Mill B V 1997 *J. Phys.: Condens. Matter*, **9**, 3833-3851
- [14] Yashima M and Komatsu T 2009 *Chem. Commun.*, 1070-1072
- [15] Delarue P, Lecomte C, Jannin M, Marnier G and Menaert B 1999 *J. Phys.: Condens. Matter*, **11**, 4123-4134
- [16] Norberg S T, Sobolev A N and Streltsov V A 2003 *Acta Crystallogr.* **B59**, 353-360
- [17] Belokoneva E L, Yakubovich O V, Tsirel'son V G and Urusov V S 1990 *Izv. Akad. Nauk SSSR Neorg. Mater.*, **26**, 595-601
- [18] Norberg S T and Ishizawa N 2005 *Acta Crystallogr.* **C61**, i99-i102
- [19] Novikova N E, Verin I A, Sorokina N I, Alekseeva O A, Voronkova V I, Tseitlin M and Roth M 2008 *Crystallogr. Rep.*, **53**, 942-951
- [20] Delarue P, Lecomte C, Jannin M, Marnier G and Menaert B 1998 *Phys. Rev. B*, **58**, 5287-5295
- [21] Thomas P A and Womersley M N 1998 *Acta Crystallogr.* **B54**, 645-651
- [22] Norberg S T, Gustafsson J and Mellander B-E 2003 *Acta Crystallogr.* **B59**, 588-595

- [23] Larsen F K 1995 *Acta Crystallogr.* **B51**, 468-482
- [24] Alekseeva O A, Dudka A P, Novikova N E, Sorokina N I, Agapova E I and Voronkova V I 2008 *Crystallogr. Rep.*, **53**, 557-564
- [25] Dudka A 2008 *J. Appl. Crystallogr.*, **41**, 83-95
- [26] Hansen N K, Protas J and Marnier G 1988 *C. R. Acad. Sci.*, **307**, 475-478
- [27] Levine B F 1973 *Phys. Rev. B*, **7**, 2600-2626
- [28] Hansen N K, Protas J and Marnier G 1991 *Acta Crystallogr.* **B47**, 660-672
- [29] Phillips M L F, Harrison W T A, Stucky G D, McCarron E M, Calabrese J C and Gier T E 1992 *Chem. Mater.*, **4**, 222-233
- [30] Mayo S C, Thomas P A, Teat S J, Loiacono G M and Loiacono D N 1994 *Acta Crystallogr.* **B50**, 655-662
- [31] Xue D and Zhang S 1999 *J. Solid State Chem.*, **142**, 156-162
- [32] Thomas P A, Baldwin A, Dupree R, Blaha P, Schwarz K, Samoson A and Gan Z H 2004 *J. Phys. Chem. B*, **108**, 4324-4331
- [33] Rietveld H M 1969 *J. Appl. Crystallogr.*, **2**, 65-67
- [34] McGreevy R L and Pusztai L 1988 *Mol. Simul.*, **1**, 359-367
- [35] McGreevy R L 2001 *J. Phys.: Condens. Matter.*, **13**, R877-R913
- [36] Jacco J C, Loiacono G M, Jaso M, Mizell G and Greenberg B 1984 *J Cryst. Growth*, **70**, 484-490
- [37] Hull S, Smith R I, David W I F, Hannon A C, Mayers J and Cywinski R 1992 *Physica B*, **180-181**, 1000-1002
- [38] Soper A K, *Gudrun – A computer program developed for analysis of neutron diffraction data*, http://www.isis.rl.ac.uk/disordered/dmgroup_home.htm
- [39] Keen D A 2001 *J. Appl. Crystallogr.*, **34**, 172-177
- [40] Tucker M G, Keen D A, Dove M T, Goodwin A L and Hui Q 2007 *J. Phys.: Condens. Matter*, **19**, art 335218
- [41] Norberg S T, Tucker M G and Hull S 2009 *J. Appl. Crystallogr.*, **42**, 179-184

- [42] Norberg S T, Ahmed I, Hull S, Marrocchelli D and Madden P A 2009 *J. Phys.: Condens. Matter*, **21**, art 215401
- [43] Brese N E and O’Keeffe M 1991 *Acta Crystallogr.* **B47**, 192-197
- [44] Larson A C and von Dreele R B *General Structure Analysis System (GSAS)*, Los Alamos National Laboratory Report LAUR 1994, 86-748
- [45] Norberg S T, Streltsov V A, Svensson G and Albertsson J 2000 *Acta Crystallogr.* **B56**, 980-987
- [46] Wells S A, Dove M T and Tucker M G 2002 *J. Phys.: Condens. Matter*, **14**, 4567-4584
- [47] Mohn C E, Stølen S, Norberg S T and Hull S. 2009 *Phys. Rev. Lett.*, **102**, 155502

Tables

Table 1

Crystallographic parameters for the Rietveld refined KTP at RT and 900°C.

	RT	900°C
Cell setting	Orthorhombic	Orthorhombic
Space group	$Pna2_1$	$Pna2_1$
a (Å)	12.80809(9)	12.9478(2)
b (Å)	6.39916(5)	6.48479(13)
c (Å)	10.58137(5)	10.54550(11)
V (Å ³)	867.260(6)	885.442(16)
R_{wp}	0.0197	0.0222
χ^2	3.326	1.214
Number of data points	3180	3180
Number of variables	56	56
Number of Bragg peaks	1899	1937
$R(F^2)_{obs}$	0.0139	0.0522

Table 2

Rietveld refined fractional coordinates and isotropic thermal vibration parameters for KTP at RT and 900°C.

	RT				900°C			
	x	y	z	u_{iso}	x	y	z	u_{iso}
K1	0.3779(4)	0.2162(6)	0.3114(3)	0.0160(5)	0.3890(14)	0.215(3)	0.3436(15)	0.073(3)
K2	0.1090(3)	0.3009(7)	0.0669(3)	= u_{K1}	0.1109(14)	0.311(4)	0.0801(18)	= u_{K1}
Ti1	0.37137(17)	0.4992(8)	0.0016(4)	0.0026(4)	0.3719(4)	0.5108(18)	0.0090(11)	0.0128(9)
Ti2	0.2451(4)	0.7341(6)	0.2513(4)	= u_{Ti1}	0.2448(8)	0.7410(18)	0.2490(11)	= u_{Ti1}
P1	0.4976(4)	0.6644(2)	0.2617(4)	0.00264(17)	0.4983(7)	0.6623(6)	0.2610(8)	0.0097(4)
P2	0.18148(11)	0.4970(8)	0.5121(4)	= u_{P1}	0.1784(3)	0.5035(14)	0.5089(9)	= u_{P1}
O1	0.4835(2)	0.5126(4)	0.1504(3)	0.00535(5)	0.4848(4)	0.5011(10)	0.1524(5)	0.02128(19)
O2	0.5091(2)	0.5345(4)	0.3846(2)	= u_{O1}	0.5080(5)	0.5435(7)	0.3878(6)	= u_{O1}
O3	0.4006(2)	0.8002(5)	0.2777(3)	= u_{O1}	0.4028(5)	0.8016(12)	0.2773(8)	= u_{O1}
O4	0.5935(2)	0.8079(5)	0.2405(3)	= u_{O1}	0.5921(6)	0.8047(13)	0.2365(8)	= u_{O1}
O11	0.2765(2)	0.5325(5)	0.1415(3)	= u_{O1}	0.2822(5)	0.5367(11)	0.1362(6)	= u_{O1}
O12	0.2258(3)	0.9572(5)	0.3888(3)	= u_{O1}	0.2297(5)	0.9503(11)	0.3854(6)	= u_{O1}
O5	0.1103(3)	0.6895(6)	0.5422(2)	= u_{O1}	0.1001(4)	0.6896(14)	0.5358(7)	= u_{O1}
O6	0.1124(3)	0.3087(6)	0.4882(3)	= u_{O1}	0.1182(4)	0.3078(11)	0.4773(6)	= u_{O1}
O7	0.2549(3)	0.4610(5)	0.6257(3)	= u_{O1}	0.2538(5)	0.4469(10)	0.6144(5)	= u_{O1}
O8	0.2511(3)	0.5394(6)	0.3973(3)	= u_{O1}	0.2446(4)	0.5345(9)	0.3875(6)	= u_{O1}

Table 3

Temperature related changes in oxygen coordination number and corresponding average bond distances around the K⁺ cations. Bond distance cut-off set to 3.30 Å.

CN	RT		300°C		500°C		700°C		900°C	
4	0.1%	2.699 Å	0.2%	2.715 Å	0.1%	2.739 Å	0.3%	2.730 Å	0.5%	2.738 Å
5	1.1%	2.801 Å	2.0%	2.798 Å	2.6%	2.798 Å	3.5%	2.805 Å	5.3%	2.813 Å
6	5.4%	2.856 Å	8.0%	2.852 Å	11.4%	2.851 Å	14.9%	2.860 Å	19.2%	2.871 Å
7	21.2%	2.871 Å	28.3%	2.876 Å	30.9%	2.880 Å	33.7%	2.897 Å	34.2%	2.910 Å
8	54.6%	2.886 Å	48.7%	2.897 Å	43.6%	2.905 Å	36.1%	2.928 Å	30.8%	2.942 Å
9	17.5%	2.945 Å	12.9%	2.949 Å	11.2%	2.954 Å	11.2%	2.966 Å	9.5%	2.975 Å
10	0.1%	2.992 Å	0.1%	2.990 Å	0.2%	2.995 Å	0.3%	3.000 Å	0.4%	3.013 Å
	7.936	2.890 Å	7.752	2.891 Å	7.621	2.893 Å	7.509	2.908 Å	7.359	2.911 Å